Nanoscale

Accepted Manuscript

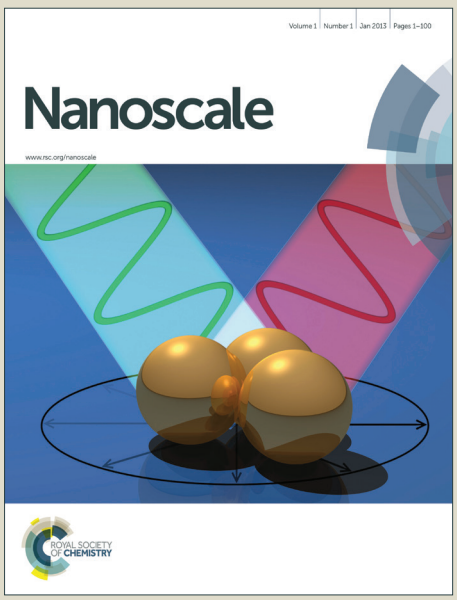

ROYAL SOCIETY OF CHEMISTRY

www.rsc.org/nanoscale

Nanoscale

RSCPublishing

COMMUNICATION

Monitoring Plasmon-Driven Surface Catalyzed Reactions in Situ Using Time-dependent Surface-Enhanced Raman Spectroscopy on Single Particle of Hierarchical Peony-Like Silver Microflower†

Cite this: DOI: 10.1039/x0xx00000x

Received 00th January 2014,
Accepted 00th January 2014

DOI: 10.1039/x0xx00000x

www.rsc.org/

Xianghu Tang,[a,b] Wenya Cai,[a] Liangbao Yang [a *] and Jinhuai Liu [a,b *]

Investigating the kinetics of catalytic reactions with surface-enhanced Raman scattering (SERS) on a single particle remains a significant challenge. In this study, the single particle of the constructed hierarchical peony-like silver microflowers (SMF) with highly roughened surface led to the coupling of high catalytic activity with a strong SERS effect, which own to an excellent bifunctional platform for in situ monitoring of surface catalytic reactions. The kinetics of the reaction of 4-nitrothiophenol (4-NTP) dimerizing into 4, 4'-dimercaptoazobenzene (DMAB) was investigated and comparative studied by using SERS technique on single particle of different morphologies of SMF. The results indicate that fully developed nanostructure of hierarchical SMF has both larger SERS enhancement and apparent reaction rate constant *k*, which may be useful for monitoring and understanding the mechanism of plasmon-driven surface catalyzed reactions.

Determining the catalytic activity and the reaction kinetics are key issues when new catalysts are developed, characterized, and introduced.[1] Infrared, ultraviolet-visible, Raman or fluorescence spectroscopy for the study of heterogeneous catalysts at work, are limited in terms of their spatial resolution to the micrometre scale. Fortunately, in recent years, by means of surface-enhanced Raman scattering (SERS), plasmon-driven surface catalyzed reactions have attracted more and more attention because they open up a new pathway for monitoring and controlling the catalyzed reactions on metallic catalysts.[2-6] However, direct observations of a catalytic process by SERS have been rare as they require bimetallic or bifuctional catalytically active nanoparticles. Only a limited number of preliminary studies can be found in the literature to date.[1, 7-9] These bifunctional nanomaterials include Au-Pd alloy horns on Au nanorods[8], Au/Pt/Au core/shell nanoraspberries composite with plasmonic (Au) and catalytic (Pt, or Pd) properties[1, 7], and a single bifunctional 3D superstructure comprising small gold satellites self-assembled onto a large shell-isolated gold core[9]. However, the complicated multistep preparation processes for these materials may result in inhomogeneous particle morphologies and hinder in-depth research on these systems as a consequence.[8]

Recently, plasmon-driven surface catalyzed reaction of 4-nitrothiophenol (4-NTP) dimerizing into DMAB has been proved using tip-enhanced Raman spectroscopy (TERS) and SERS techniques.[10-16] It is experimentally investigated substrate-, wavelength-, and time-dependent plasmon-assisted surface photocatalyzed reactions of 4-NTP dimerizing into DMAB on Au, Ag, and Cu films.[17] None of these studies goes as far as studying directly the kinetics of a catalytic reaction in situ using spatiotemporal SERS on a single particle. In order to study directly the kinetics of plasmon-driven this chemical reaction in situ, the versatility, stability, and general applicability of a simple particle is needed that plasmonic properties and also act as a catalyst. Integrating high SERS and catalytic activity into a simple particle through facile synthesis, which requires a rational design that takes particle size, shape, composition, and nanoscale architecture into account, remains challenging.

Table 1 Samples obtained under different experimental conditions

Sample number	0.06 M CH_3COOAg/mL	0.12 M NH_2OH/mL	Particle size/ d_{50}*, μm
SMF-1	1.0	1.0	2.0
SMF-2	1.0	2.0	2.3
SMF-3	1.0	3.0	2.6
SMF-4	1.0	5.0	2.8

* d_{50} is the medium diameter of the particles.

a Institute of Intelligent Machines, Chinese Academy of Sciences, Hefei 230031, China. Fax: (+86)551-65592420; E-mail: lbyang@iim.ac.cn, jhliu@iim.ac.cn
b University of Science and Technology of China, Hefei 230026, PR China

† Electronic Supplementary Information (ESI) available: Fig.S1~S12. See DOI: 10.1039/b000000x/

Herein, we designed a facile method to synthesize monodisperse and hierarchical peony-like silver microflowers (SMF) assembled by nanostructures with tailored surface topographies in the absence of any other surfactants. Size as well as the surface roughness of the SMF can be well controlled. It is very importance that such a bifunctional platform offers a unique opportunity to investigate the intrinsic reaction kinetics on the catalyst surface by excluding the influence of adsorption/desorption of reactants and products.

The morphologies of the samples were characterized by SEM. As shown in Fig.1, monodisperse particles with uniform size and well defined surface topographies were obtained through our synthesis route. Typically, from Fig.1C$_1$, it shows the low-magnification SEM image of sample obtained by reducing 1.0 mL of 0.06 M CH_3COOAg with 3.0 mL of 0.12 M NH_2OH solution. It is clearly revealed that the products consist almost entirely of monodisperse peony-like silver nanostructure, and inset of Fig.1C$_1$ illustrates that most particles size were about 2~3 μm with narrow size distribution. The corresponding higher-magnification SEM image shown in Fig.1C$_2$ further indicates that the samples are composed of several aggregated petals with about 80±20 nm thick. To obtain more information of the tailoring process, a group of parallel experiments were carried out and the experimental conditions were collected in Table 1. It is verified that the amount of the NH_2OH plays a vital role in the hierarchical structure of the SMF. By adjusting the ratio between the amount of

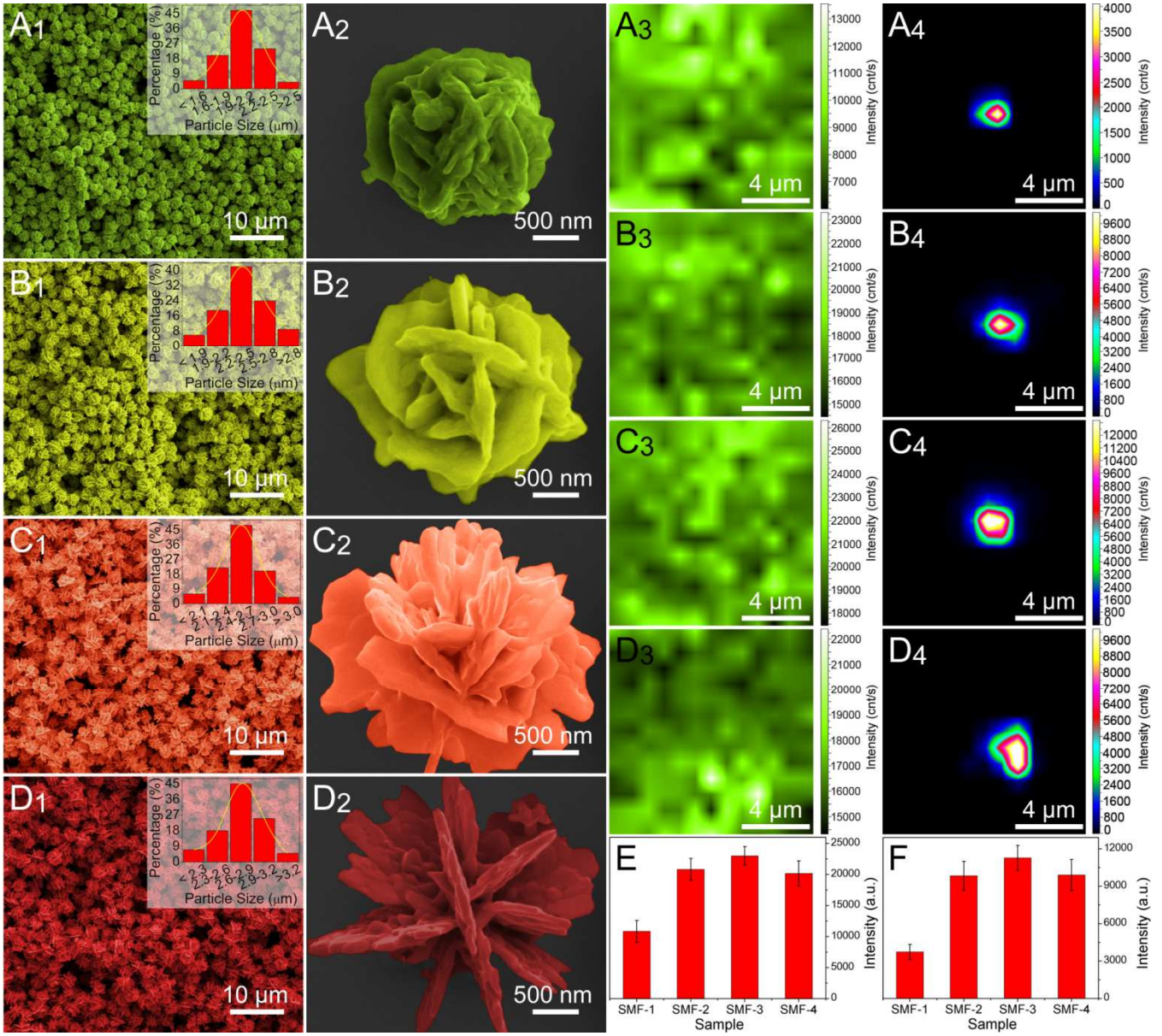

Fig.1 Typical SEM images and SERS mapping of hierarchical silver microflowers synthesized under different conditions. (A_1-D_1) SEM images of sample SMF-1, 2, 3, & 4 aggregated on a silicon wafer, respectively. Insets in panel (A_1-D_1) show the corresponding particle size distribution of as-synthesized samples. (A_2-D_2) Magnified SEM images for single particles of SMF-1, 2, 3, & 4, respectively. (A_3-D_3) and (A_4-D_4) color-coded area SERS mapping of the aggregates (12 μm × 12 μm) and single particles of SMF-1, 2, 3, & 4, respectively. (E) and (F) the average SERS enhancement of aggregates and single particles, respectively (more details can be seen in Fig.S3, ESI†). All SERS performance based on the intensity of the spectral band at ~1176 cm^{-1} of CV. The spectra were collected with 1 s integration time, and a laser power of 2 mW at 632.8 nm laser excitation.

the two reactants, particle size as well as the surface topographies of the products can be well controlled. From Table 1 and Fig.1, we can get that small amount of NH_2OH conduced to silver structure grow into flower bud (Fig.1A_2, B_2) and the formation of nano-petal like texture was not fully developed. With the increases of the amount of NH_2OH, it was obvious to see that the buds blossomed into flowers (Fig.1C_2, D_2), meanwhile, the particle sizes became larger. The proposed reason for this phenomenon was that nucleus grew more quickly in large amount reducing agent reaction system. The results of X-ray diffractometer (XRD) patterns (Fig.S1, ESI†), TEM and the corresponding energy dispersive spectroscopy (EDS), and selected area electron diffraction (SAED) pattern (Fig.S2, ESI†), show that pure and silver crystals were formed.

The SERS properties of SMF were evaluated by using crystal violet (CV) as probe molecules. Those nanostructures can allow one single particle acting as SERS substrates for sensing and imaging applications (Fig.S3, ESI†). The SERS mapping of single particle and aggregates were evaluated based on the intensity of the spectral band at 1176 cm^{-1} of 10^{-7} M CV (typical spectral band of CV can be seen in Fig.S4, ESI†).[18-20] Fig.1A_3-D_3 shows SERS mapping of aggregates of the products synthesized under different conditions. It can be found that the SMF-3 exhibits the highest enhancement efficiency for the two neighbouring nano-petals can form a wedge-shaped architecture which is beneficial to trap and capture probing molecules[21-23] for improving the SERS performances, as shown in Fig.1E. Importantly, SERS mapping studies of single particles reveal the same tendency. However, further comparative study between Fig.1E and F, it can be found that the average SERS enhancements for aggregates exceed the corresponding single particles by 2~3 times. This phenomenon can be explained that those nanostructure particle interactions in the aggregates resulting in additional "hot spots".[24] From the mentioned above, it is evident that, as the surface topography of particle changed to the more complex one with the nanostructure full developed, the larger SERS enhancement appeared. But as overgrowth of nano-petal like texture developed, e.g. sample of SMF-4, SERS efficiency trend to decrease to some extent. Thus, as a single particle, which slightly larger than the spot sizes of the laser beam focused on the substrate, with large SERS enhancement can be easily spotted under an optical microscope, it can be used to monitor plasmon-driven surface catalyzed reaction with no noise from surrounding environments that are normally present on a flat substrate.

In this study, we investigated the photocatalytic activity on a single SMF particle using the reduction of 4-NTP to DMAB as a model reaction.[10, 25] Fig.2A illustrates the principle to monitor the reaction on a single SMF particle using SERS technique. Firstly, a droplet of solution containing SMF and 10^{-5} M 4-NTP was aged for ~1 h. After adsorption of 4-NTP, the substrates were rinsed and diluted with ethanol and dispersed on a silicon wafer. And then, time-dependent SERS spectra on a single particle under continuous laser excitation were carried out. Initially, the SERS spectrum exhibits bands characteristic of 4-NTP,[1, 25] just as shown in Fig.2B, $\nu(-NO_2)$ stretching mode of 4-NTP at 1345 cm^{-1} can clearly be seen. Time-dependent SERS spectra (Fig.S5, ESI†) and color-coded intensity 3D SERS mapping in the frequency range of 1100cm^{-1} to 1700 cm^{-1} were taken under 632.8 nm laser excitation for a laser power of 0.36 mW, as can be seen from Fig.2D. With increasing the laser exposure time, the $\nu(-NO_2)$ peak of 4-NTP decreases, while peaks at 1142 cm^{-1} due to β(CH), 1390 and 1436 cm^{-1} due to ν(-N=N-) that are related to DMAB increase in intensity, indicating the gradual conversion of 4-NTP to DMAB. After continuous laser excitation, the $\nu(-NO_2)$ peak of 4-NTP completely disappears, and the Raman spectrum is dominated by the peaks at 1142, 1390 and 1436 cm^{-1}, which means that all 4-NTP molecules have been dimerized into DMAB,[2, 11, 25] as shown in Fig.2C Here, it should be note that long hours laser excitation can cause the decrease of intensity of SERS peaks to some extent (Fig.S5B, ESI†) for long hours laser excitation on SMF surface may induce probe molecules consumption. Besides, we also find that even few minutes laser excitation with 632.8 nm for a higher power or 532 nm can cause the decrease of intensity of SERS peaks dramatically (Fig.S6, S7, ESI†). Furthermore, no spectral changes were observed in a control experiment using 4-NTP in the absence of SMF (Fig.S8, ESI†). In addition, we carried out another control experiment by adsorbing 4-NTP molecules on SMF for different ageing time in dark environment, and then measured the SERS signals (Fig.S9, ESI†). From the results, it can be found that only SERS signals of 4-NTP but no signals of DMAB can be observed even for ageing 36 h. Therefore, we can get that the conversion of 4-NTP to DMAB requires SERS active metal materials, appropriate laser excitation and time.[10, 11]

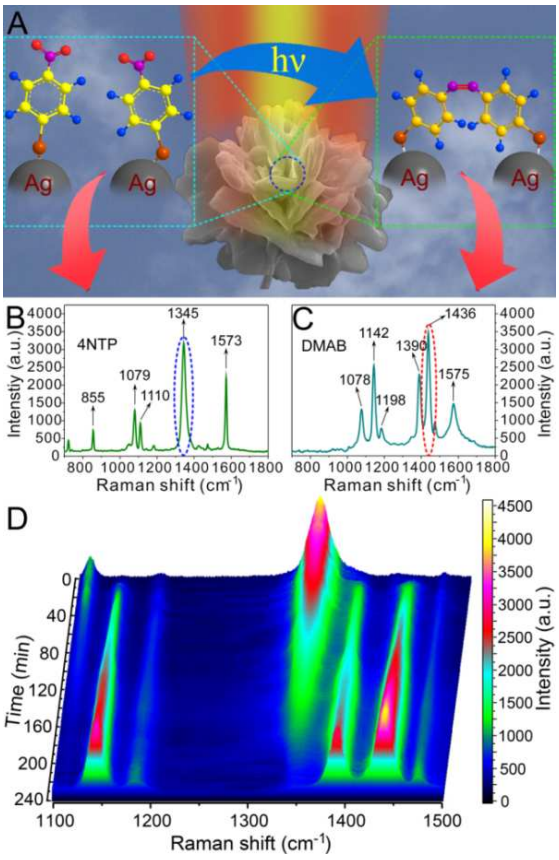

Fig.2 (A) Schematic illustration of plasmon-driven surface catalyzed reaction of 4-NTP dimerizing into DMAB monitored by single particle SERS substrate. (B&C) SERS spectra of 4-NTP and DMAB. (D) Color-coded intensity of spatiotemporal SERS mapping under continuous 632.8 nm laser excitation. The spectra were collected for a single particle of SMF-3 with an integration time of 1 s, and a laser power of 0.36 mW.

To further monitor the reaction over time, the kinetics of the reaction of 4-NTP dimerizing into DMAB were investigated and comparative studied by using SERS technique on single particle of different substrates. As no any other agent was used, as well as continuous illumination and laser excitation, and according to the chemical equation (1), it can be assumed that the reaction can be monitored by using second-order chemical kinetics[26-28] to understand the dimerization process. For this, equation (2) can be used to determine the second-order reaction rate constant, k_0, where a represents the initial concentration of 4-NTP adsorbed on silver microflowers, x is the concentration of DMAB that were reacted at time t, and a-$2x$ represents the concentration of unreacted 4-NTP that remain at time t. Specifically, the reaction rate constant k_0 can be determined as follows.

$$2HSC_6H_4NO_2\ (R) \xrightarrow{h\nu} HSC_6H_4N{=}\ NC_6H_4SH\ (P) \quad (1)$$

t=0	a	0
t=t	a-$2x$	x

$$\frac{dx}{dt} = k_0(a-2x)^2 \quad (2)$$

$$\int_0^x \frac{dx}{(a-2x)^2} = \int_0^t k_0 dt \quad (3)$$

Integrating this for the boundary conditions t=0 to t=t and x_t=0 to x_t=x, gives:

$$\frac{x}{a-2x} = ak_0t \quad (4)$$

Generally, the peak intensity ($I_{SERS,\ R}$ and $I_{SERS,\ P}$) of SERS spectrum is proportional to the concentration (a-$2x$ and x) of the probe[29-31], i.e., a-$2x$ $\propto I_{SERS,\ R}$, $x \propto I_{SERS,P}$. Therefore, we can get the equality as follows:

$$\frac{x}{a-2x} \propto \frac{I_{SERS,P}}{I_{SERS,R}} \quad (5)$$

or $$\frac{I_{SERS,P}}{I_{SERS,R}} = kt \quad (k \propto ak_0) \quad (6)$$

Here R and P represent the reactant 4-NTP and the product DMAB, respectively. $I_{SERS,P}$ and $I_{SERS,R}$ are the intensities of the bands at 1436 cm^{-1} of DMAB and 1345 cm^{-1} of 4-NTP, respectively. Under the condition of a given initial concentration of starting material, the apparent rate constant k is proportional to the reaction rate constant, k_0. Thus, from Equation (6), it can be found that the changes of the intensity of the typical DMAB band at 1436 cm^{-1} relative to the intensity of 4-NTP band at 1345 cm^{-1} could be used for relative quantitation the reaction rate. Fig.3 illustrated the corresponding plot of $I_{SERS,\ P}/I_{SERS,\ R}$ versus reaction time t, in which curve (I), (II), (III) and (IV) are the records for the single particles of SMF-1, 2, 3 and 4 as the substrates, respectively. The results show that, since the relative concentrations of 4-NTP are the same in all experiments, the apparent rate constants of the reactions catalyzed by SMF-1 and 2 are somehow smaller than those obtained by SMF-3 and 4, giving k_{SMF-1} =(4.330± 0.045)×10^{-3} min^{-1}, k_{SMF-2}=(5.680±0.049)×10^{-3} min^{-1}, k_{SMF-3}= (6.340±0.058)×10^{-3} min^{-1}, and k_{SMF-4}=(6.270±0.083)×10^{-3} min^{-1}, respectively. One reason for this phenomenon could be that the sample of SMF-3 and 4 have more fully developed nanostructure, which is propitious to the catalyzed reaction (Fig.S10, ESI†). Another suggestion could be the optical absorption and SERS properties of the nano-petal like texture from the SMF would also have an impact on the detection in kinetic studies based on SERS technique. From Fig.3, it can be found that when we prolonged the reaction times, the reactions maintain equilibrium, and then decrease for long hour's laser excitation on SMF surface may induce probe molecules consumption. These results demonstrate that the conversions of 4-NTP to DMAB are substrate-, and time-dependent plasmon-driven surface photocatalyzed reactions.[17] Additionally, the kinetic study using another two samples of SMF-3 platforms are repeated (Fig.S11, ESI†), and the apparent rate constants determined from two independent experiments accord closely with each other, showing the reliability of this method for kinetics study. These results clearly demonstrate that the kinetic parameters determined with this method are intrinsic, and provide strong evidence for the reliability of our conclusions on the reaction kinetics. Meanwhile, FTIR characterization has been presented, and which also shows that the conversion of 4-NTP to DMAB (Fig.S12, ESI†), but it is difficult for FTIR technique to monitor plasmon-driven surface catalyzed reactions in situ on single particle of hierarchical peony-like silver microflower. At last, it should be noted that the validity of our method is based on two prerequisites: (i) 4-NTP molecules form a uniform monolayer on a single SMF particle surface, which is well characterized and generally accepted. (ii) For the second-order chemical kinetics, the apparent rate constant k is proportional to the reaction rate constant, k_0, which can actually be determined from the SERS intensities of $I_{SERS,\ P}/I_{SERS,\ R}$ versus reaction time t. Importantly, we prefer to use SERS intensities is proportional to the concentration of reactant and product.

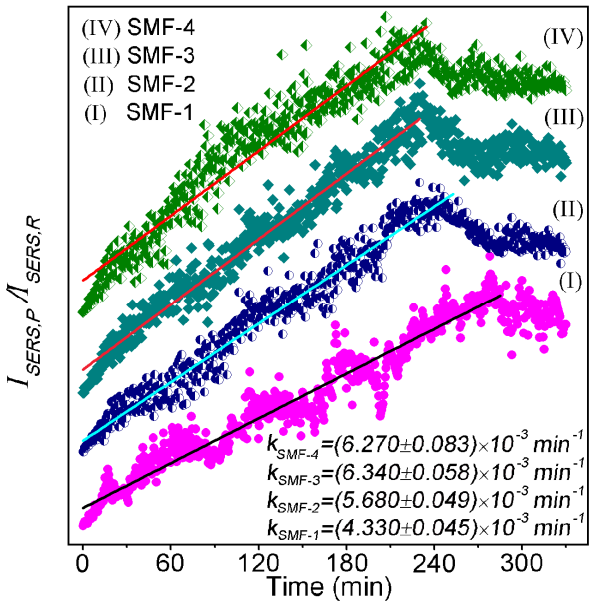

Fig.3 Determination of the apparent rate constant for the plasmon-driven surface catalyzed reactions of 4-NTP dimerizing into DMAB with different substrates: (I) SMF-1, (II) SMF-2, (III) SMF-3, and (IV) SMF-4.

Conclusions

In summary, the designed and prepared hierarchical SMF performed satisfying SERS properties for single particle SERS substrate for monitoring the plasmon-driven surface catalyzed reaction of 4-NTP dimerizing into DMAB. By adjusting the ratio between the amount of NH_2OH and CH_3COOAg solution, size as well as the surface roughness

of the SMF can be well controlled. In particular, we have obtained hierarchical peony-like SMF with fully developed nano-petal structure, which exhibits good SERS activity as SERS substrate as well as excellent photocatalytic performance, thereby generating a nanostructured surface with both plasmonic and catalytic properties. Besides, we have demonstrated that the kinetics of plasmon-driven surface catalyzed reactions of 4-NTP dimerizing into DMAB can be real-time monitored by in situ using SERS technique on a single particle of hierarchical peony-like SMF. Moreover, the results of comparative study indicate that fully developed nanostructure of SMF has larger apparent rate constant *k*, which is helpful to understand the mechanism plasmon-driven surface catalyzed reactions. In addition, the introduction of the concept of apparent rate constant has further enabled us to compare reaction rate of the second order reactions or even different catalytic systems and the underlying kinetics such as the formation of the active species.

Acknowledgements

This work was supported by the National Basic Research Program of China (2011CB933700), the National Instrumentation program of China (2011YQ0301241001 and 2011YQ0301241101).

References

1. V. Joseph, C. Engelbrekt, J. Zhang, U. Gernert, J. Ulstrup and J. Kneipp, *Angew. Chem. Int. Ed.*, 2012, **51**, 7592-7596.
2. M. Sun and H. Xu, *Small*, 2012, **8**, 2777-2786.
3. Y. Fang, Y. Li, H. Xu and M. Sun, *Langmuir*, 2010, **26**, 7737-7746.
4. V. Canpean, M. Iosin and S. Astilean, *Chem. Phys. Lett.*, 2010, **500**, 277-282.
5. D. Wu, L. Zhao, X. Liu, R. Huang, Y. Huang, B. Ren and Z. Tian, *Chem. Commun.*, 2011, **47**, 2520-2522.
6. M. Sun, Y. Hou, Z. Li, L. Liu and H. Xu, *Plasmonics*, 2011, **6**, 681-687.
7. W. Xie, C. Herrmann, K. Kompe, M. Haase and S. Schlucker, *J. Am. Chem. Soc.*, 2011, **133**, 19302-19305.
8. J. F. Huang, Y. H. Zhu, M. Lin, Q. X. Wang, L. Zhao, Y. Yang, K. X. Yao and Y. Han, *J. Am. Chem. Soc.*, 2013, **135**, 8552-8561.
9. W. Xie, B. Walkenfort and S. Schluecker, *J. Am. Chem. Soc.*, 2013, **135**, 1657-1660.
10. E. M. v. S. Lantman, T. Deckert-Gaudig, A. J. G. Mank, V. Deckert and B. M. Weckhuysen, *Nat. Nanotechnol.*, 2012, **7**, 583-586.
11. L. L. Kang, P. Xu, B. Zhang, H. H. Tsai, X. J. Han and H. L. Wang, *Chem. Commun.*, 2013, **49**, 3389-3391.
12. L. L. Kang, P. Xu, D. T. Chen, B. Zhang, Y. C. Du, X. J. Han, Q. Li and H. L. Wang, *J. Phys. Chem. C*, 2013, **117**, 10007-10012.
13. P. Xu, L. Kang, N. H. Mack, K. S. Schanze, X. Han and H. L. Wang, *Scientific Reports*, 2013, **3**, 2997.
14. L. Zhao, M. Zhang, Y. Huang, C. T. Williams, D. Wu, B. Ren and Z. Tian, *The Journal of Physical Chemistry Letters*, 2014, 1259-1266.
15. Z. Zhang, M. Sun, P. Ruan, H. Zheng and H. Xu, *Nanoscale*, 2013, **5**, 4151-4155.
16. Z. Zhang, L. Chen, M. Sun, P. Ruan, H. Zheng and H. Xu, *Nanoscale*, 2013, **5**, 3249-3252.
17. B. Dong, Y. Fang, X. Chen, H. Xu and M. Sun, *Langmuir*, 2011, **27**, 10677-10682.
18. W. Meng, F. Hu, L.-Y. Zhang, X.-H. Jiang, L.-D. Lu and X. Wang, *Journal of Molecular Structure*, 2013, **1035**, 326-331.
19. S. L. Kleinman, E. Ringe, N. Valley, K. L. Wustholz, E. Phillips, K. A. Scheidt, G. C. Schatz and R. P. Van Duyne, *J. Am. Chem. Soc.*, 2011, **133**, 4115-4122.
20. M. V. Canamares, C. Chenal, R. L. Birke and J. R. Lombardi, *J. Phys. Chem. C*, 2008, **112**, 20295-20300.
21. M. F. Zhang, A. W. Zhao, H. Y. Guo, D. P. Wang, Z. B. Gan, H. H. Sun, D. Li and M. Li, *Crystengcomm*, 2011, **13**, 5709-5717.
22. H. Liang, Z. Li, W. Wang, Y. Wu and H. Xu, *Adv. Mater.*, 2009, **21**, 4614-4618.
23. F. Zhang, P. Chen, X. Li, J. T. Liu, L. Lin and Z. W. Fan, *Laser Physics Letters*, 2013, **10**.
24. J. Fang, S. Du, S. Lebedkin, Z. Li, R. Kruk, M. Kappes and H. Hahn, *Nano Lett.*, 2010, **10**, 5006-5013.
25. L. Zhao, Y. Huang, X. Liu, J. R. Anema, D. Wu, B. Ren and Z. Tian, *Phys. Chem. Chem. Phys.*, 2012, **14**, 12919-12929.
26. K. J. Laidler, *Chemical kinetics, 3rd edition*, Harper and Row Publishers Inc, New York 1987.
27. S. T. S. Joseph, B. I. Ipe, P. Pramod and K. G. Thomas, *J. Phys. Chem. B*, 2006, **110**, 150-157.
28. M. Sethi and M. R. Knecht, *Langmuir*, 2010, **26**, 9860-9874.
29. G. H. Gu and J. S. Suh, *J. Phys. Chem. A*, 2009, **113**, 8529-8532.
30. D. K. Lim, K. S. Jeon, J. H. Hwang, H. Kim, S. Kwon, Y. D. Suh and J. M. Nam, *Nat. Nanotechnol.*, 2011, **6**, 452-460.
31. W. Ren, Y. X. Fang and E. K. Wang, *Acs Nano*, 2011, **5**, 6425-6433.